

## Influence of Alkali Metal Cations upon the Kolbe–Schmitt Reaction Mechanism

Zoran Marković,<sup>†</sup> Svetlana Marković,<sup>\*,‡</sup> and Nebojša Begović<sup>§</sup>

Faculty of Agronomy, University of Kragujevac, 34 Cara Dušana, 32000 Čačak, Serbia and Montenegro,  
 Faculty of Science, University of Kragujevac, 12 Radoja Domanovića, POB 60, 34000 Kragujevac, Serbia  
 and Montenegro, and Holding Institute of General and Physical Chemistry, 12/V Studentski trg,  
 11000 Belgrade, Serbia and Montenegro

Received February 20, 2006

The mechanisms of the carboxylations of lithium, potassium, rubidium, and cesium phenoxides are investigated by means of the DFT method with the LANL2DZ basis set. It is shown that the reactions of all alkali metal phenoxides with carbon dioxide occur via very similar reaction mechanisms. The reactions can proceed in the ortho and para positions. The exception is lithium phenoxide which yields only salicylic acid in the Kolbe–Schmitt reaction. It is found that the yield of the para substituted product increases with increasing the ionic radius of the alkali metal used. An explanation for this experimental and theoretical observation is proposed.

## INTRODUCTION

The Kolbe–Schmitt reaction is a carboxylation reaction of alkali metal phenoxides with carbon dioxide where hydroxybenzoic acids are formed.<sup>1–3</sup> This reaction has been used for more than a century for industrial production of aromatic hydroxy acids, such as salicylic acid, *p*-hydroxybenzoic acid, 3-hydroxy-2-naphthoic acid, 6-hydroxy-2-naphthoic acid, etc. These acids play a significant role in the synthesis of numerous products, such as pharmaceuticals, antiseptic, fungicidal and color-developing agents, textile assistants, polyesters, high-polymeric liquid crystals, and dyes.<sup>4,5</sup> The general outline of the reaction is presented in Figure 1.

The Kolbe–Schmitt reaction is a classical example of a reaction in which the nature of the reaction products is dependent on the alkali metal cation. For example, under comparable conditions, lithium and sodium phenoxides yield salicylic acid as the major product,<sup>7</sup> whereas potassium, rubidium, and cesium phenoxides yield the mixtures of salicylic and *p*-hydroxybenzoic acids in different ratios.<sup>6,7</sup> It was found that, in the carboxylation reaction of potassium phenoxide at higher constant pressures, the yield of the para product decreased with increasing temperature.<sup>7</sup> On the other hand, in the same reaction under atmospheric pressure, the yield of the para product increased with increasing temperature. In the case of rubidium phenoxide, the yields of the ortho and para products were almost constant under constant pressure and at the temperature in the range of 150–200 °C.<sup>8</sup> In the carboxylation of cesium phenoxide at the temperatures of 150, 200, and 260 °C at constant pressure, the yield of the para product decreased with increasing temperature.<sup>8,9</sup>

Unfortunately, the experimental data representing the distribution of products of the carboxylation reactions of

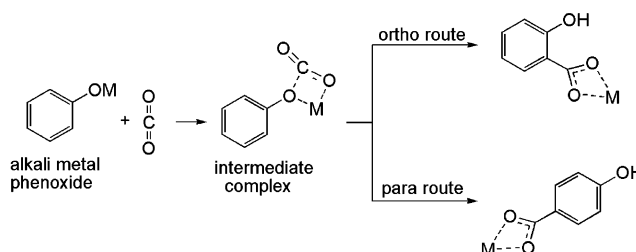


**Figure 1.** Reaction scheme for the Kolbe–Schmitt reaction. M represents alkali metals.

different alkali metal phenoxides at a certain constant conditions of temperature, pressure, and reaction time are not available. Table 1 shows the distribution of the ortho and para products of the Kolbe–Schmitt reaction of different alkali metal phenoxides at relatively similar experimental conditions.

Despite the inconsistency of the experimental conditions, one can observe that the yield of *p*-hydroxybenzoic acid generally increases with an increasing ionic radius of the alkali metal.

The aim of this work is to investigate the dependence of the distribution of products of the Kolbe–Schmitt reaction on the alkali metal cation. For this purpose, the Kolbe–Schmitt reaction mechanism is investigated for different alkali metal phenoxides (i.e. lithium, potassium, rubidium, and cesium phenoxides) by means of the DFT method. Particular attention is devoted to the reaction steps which determine the distribution of products.

## BACKGROUND OF THE KOLBE–SCHMITT REACTION MECHANISM

There are controversial discussions concerning the mechanism of the Kolbe–Schmitt reaction. Kolbe, Schmitt, and Hentschel<sup>1–3,7</sup> supposed that the reaction proceeded via an intermediate alkali metal phenyl carbonate (PhO–CO<sub>2</sub>Na). Tijmstra<sup>10</sup> supposed that the decarboxylation occurred at the

\* Corresponding author e-mail: mark@kg.ac.yu.

<sup>†</sup> Faculty of Agronomy, University of Kragujevac.

<sup>‡</sup> Faculty of Science, University of Kragujevac.

<sup>§</sup> Holding Institute of General and Physical Chemistry.

**Table 1.** Carboxylation of Alkali Metal Phenoxides under Relatively Comparable Conditions

alkali metal phenoxide	temp (°C)	pressure (atm)	reaction time (h)	ortho/para ratio
lithium phenoxide <sup>7</sup>	200	8	18	1:0
sodium phenoxide <sup>6</sup>	150	80–130	4–24	1:0.02
potassium phenoxide <sup>7</sup>	180	40	4	1:0.03
rubidium phenoxide <sup>9</sup>	150	50	1	1:1.29
cesium phenoxide <sup>9</sup>	150	50	1	1:2.32

temperatures above 80 °C and that, on increasing the temperature, a direct carboxylation of the benzene ring took place. Tijmstra did not explain the high selectivity of the reaction of sodium phenoxide and carbon dioxide. Johnson and Luttringhaus<sup>7,11</sup> assumed that the reaction occurred via cyclic stages that led to an ortho substitution. Daives<sup>12</sup> supported the idea of the formation of the complex at 80 °C and subsequent rearrangement reaction of the intermediate to salts of hydroxy aromatic acids. The evidence of the formation of a weak chelate complex between sodium phenoxide and carbon dioxide was found by means of infrared absorption spectra.<sup>13</sup> Hales assumed that the Kolbe–Schmitt reaction occurred via this intermediate complex, involving an intramolecular rearrangement with displacement of the ortho-hydrogen by electrophilic attack.<sup>13</sup> The structure of the intermediate complex suggested by Hales has not been experimentally confirmed. Ayres<sup>14</sup> supposed that the chelate complex further rearranged into a  $\pi$ -complex with C-alkylation in the ortho position, which was followed by proton transfer to the phenolic oxygen.

The work of Kunert<sup>15</sup> provided valuable information on the mechanism of the Kolbe–Schmitt reaction. On the basis of FT-IR spectra and DTA analysis the presence of the intermediate NaOPh–CO<sub>2</sub> complex was confirmed. It was also found that the complex changed to a further intermediate at increased temperature (75–80 °C). It was concluded that a direct carboxylation could be excluded from the Kolbe–Schmitt reaction mechanism.

Kosugi<sup>16</sup> investigated the Kolbe–Schmitt reaction mechanism of phenol and 2-naphthol. It was concluded, on the basis of C-13 NMR and MOPAC/PM3 calculations, that a direct carboxylation of phenoxide with carbon dioxide took place, and NaOPh–CO<sub>2</sub> was not an intermediate in the reaction. This study was focused on the carbonation of potassium phenoxide, and an exact mechanism of the reaction was not put forward.

The mechanism of the Kolbe–Schmitt reaction has been a subject of theoretical investigations, too.<sup>17–19</sup> A DFT study on the mechanism of the reaction between sodium phenoxide and carbon dioxide was performed by means of the Gaussian 98 software package at the B3LYP level of theory with the LANL2DZ basis set.<sup>17</sup> A mechanism including three transition states and three intermediates was proposed. A quantitative explanation for the low yield of *p*-hydroxybenzoic acid and the equilibrium behavior of the Kolbe–Schmitt reaction was provided. To investigate solvent effects on the Kolbe–Schmitt reaction kinetics Stanescu et al.<sup>18</sup> and Achenie et al.<sup>19</sup> performed theoretical DFT studies, where the Jaguar 4.2 program package<sup>20</sup> at the B3LYP level of theory was used. After a series of tests with different basis sets, LAV3P\*\* was selected for the calculations, taking into account the tradeoff between accuracy and computational

effort. The investigations of Achenie and Stanescu confirmed the mechanism proposed in ref 17.

In this work we find out that the Kolbe–Schmitt reaction of different alkali metal phenoxides conforms to a mechanism very similar to that of sodium phenoxide.<sup>17–19</sup> The mechanism of the carboxylation reaction of lithium phenoxide is somewhat different from those of all other alkali metal phenoxides.

## COMPUTATIONAL METHODS

Geometrical parameters of all stationary points and transition states for the reactions of alkali metal phenoxides and carbon dioxide are optimized in a vacuum, employing analytic energy gradients by means of the Becke-type three-parameter hybrid combined with the gradient-corrected correlation functional of Lee, Yang, and Parr.<sup>21,22</sup> This functional, commonly known as B3LYP,<sup>22,23</sup> implemented in the GAUSSIAN98 program package,<sup>24</sup> turned out to be quite reliable for geometrical optimizations.<sup>25</sup> All theoretical calculations are carried out by employing the LANL2DZ<sup>26–28</sup> basis set, because it proved to be reliable and reproducible for the investigations of the Kolbe–Schmitt reaction mechanism.<sup>17–19</sup> The first row atoms are described by the double- $\zeta$  basis Dunning-Hay.<sup>29</sup> The LANL2DZ basis set also includes effective core potentials used to include some relativistic effects for alkali metals from potassium to cesium. The vibrational analysis and the natural bond orbital (NBO) analysis<sup>30,31</sup> are performed for all structures at the B3LYP/LANL2DZ level. All the fully optimized transition state structures are confirmed by the existence of a sole imaginary frequency, whereas the optimized intermediate structures possess only real frequencies.

The analysis of the vibrational frequencies is performed by means of the Molden program, version 3.7.<sup>32</sup>

## RESULTS AND DISCUSSION

Before we present our results we need to fix the notation used in this work. As much as possible, we follow the notation used in refs 17–19. Since the present work is a systematic study of the carboxylation reactions of different alkali metal phenoxides (i.e. lithium, potassium, rubidium, and cesium phenoxides) in both ortho and para positions, some new symbols need to be introduced.

As it will be shown in the text that follows, the reactions of carbon dioxide with all alkali metal phenoxides under consideration occur via very similar reaction mechanisms. For this reason, we need to introduce general symbols to denote participants in a carboxylation reaction of an arbitrary alkali metal phenoxide, where the properties of these arbitrary participants can be generalized to those of corresponding participants in the carboxylation reactions of all other alkali metal phenoxides. Our notation is illustrated with Figure 2.

To distinguish differences that appear in the carboxylation reactions of different alkali metal phenoxides, i.e., to represent specific participants in the Kolbe–Schmitt reaction, we add chemical symbols of alkali metals to certain general symbols presented in Figure 2. It will be shown later that the reaction between PhO–Li and carbon dioxide does not take place in the para position. This implies that M in the symbols pTS1–M, pC–M, pTS2–M, pD–M, and pTS3–M does not cover Li.

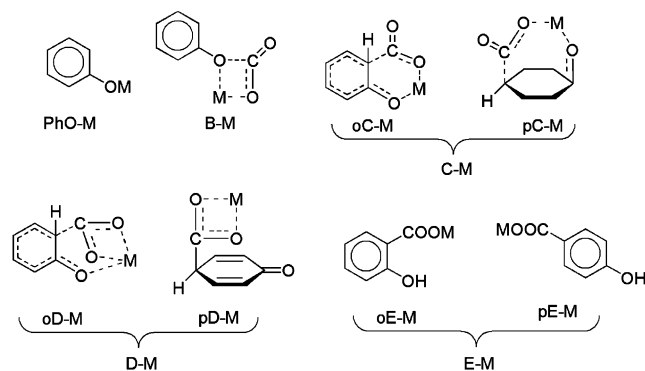


**Figure 2.** Molecular structure of the reactants, intermediates, and products studied in this work. M denotes any alkali metal under consideration (i.e. lithium, potassium, rubidium, and cesium). PhO–M, B–M, C–M, D–M, and E–M stand for alkali metal phenoxide, first intermediate, second intermediate, third intermediate, and alkali metal salt of hydroxybenzoic acid, respectively. Analogously, the symbols TS1–M, TS2–M, and TS3–M denote the first, second, and third transition states. Prefixes o and p denote ortho and para routes of the Kolbe–Schmitt reaction.

### THE MECHANISM

The mechanism of the reaction of carbon dioxide with PhO–M is examined. A direct carboxylation of benzene ring is investigated by performing a forced attack of carbon dioxide to the ortho, meta, and para positions of PhO–M. As in the case of the reaction of sodium phenoxide with carbon dioxide<sup>17–19</sup> this attack does not reveal any possible reaction path. On the other hand, a stable intermediate complex B–M is formed by approaching the reactants to each other. This step of the reaction proceeds smoothly, with the stabilization of the system, and without any activation barrier. This is in agreement with the finding that not all chemical reactions proceed via transition states, particularly in the gas phase.<sup>33</sup> The existence of the intermediate B–M in the Kolbe–Schmitt reaction has been confirmed experimentally.<sup>13,15,16</sup> This reaction path is supported by theoretical results, as follows.

In Figure 3 the HOMOs and LUMOs of PhO–K and carbon dioxide are depicted. By inspecting the HOMOs and LUMOs of all other PhO–Ms one can conclude that their shapes are very similar to those of PhO–K. The LUMO of PhO–M is located on the metal, whereas the HOMO of carbon dioxide is located on both oxygens. The HOMO of PhO–M is delocalized over the ortho and para carbons and oxygen. The LUMO of carbon dioxide is delocalized over all atoms, but the greatest contribution to the LUMO comes from the carbon atom.

The APT (atomic polar tensors) charge distribution<sup>34</sup> of the reactants (Table 2) shows that in PhO–M the positive charge is located on the metal, whereas the negative charge is distributed among the oxygen and ortho and para carbons of the benzene ring.

Both HOMO–LUMO and charge distribution analyses undoubtedly indicate that the oxygen of carbon dioxide will bond to the alkali metal, and the carbon of carbon dioxide will bond to the adjacent oxygen of PhO–M, thus forming the intermediate B–M. The geometries of all B–Ms are calculated, and it is found out that they are very similar to that reported in ref 17. It will be shown later that

the formation and geometry of B–M are not responsible for the distribution of products. For these reasons the geometries of B–Ms considered in this work are not presented.

Now, the intermediate complex undergoes further conversion. A direct carboxylation with another molecule of carbon dioxide is examined, but this attack does not reveal any possible reaction path. On the other hand, Table 2 clearly reveals that the carbon of the CO<sub>2</sub> moiety in B–M is strongly electrophilic, indicating that an electrophilic attack of the CO<sub>2</sub> moiety to the benzene ring can be expected as a plausible step of the reaction. For this reason the reaction paths for electrophilic attacks of this carbon to the ortho, meta, and para positions of B–M are examined. The meta route is not revealed. This finding is in agreement with Table 2 which shows that the ortho and para carbons in the benzene ring are nucleophilic. In addition, the greatest contribution to the HOMO of B–M comes from the ortho and para carbons of the benzene ring, indicating the sites of the electrophilic attack of the CO<sub>2</sub> moiety.

The reactions of B–M in the ortho and para positions proceed via transition states oTS1–M and pTS1–M, with the formation of the intermediates oC–M and pC–M. An exception is a conversion of B–Li, where a reaction path for an attack in the para position is not revealed. The optimized geometries for oTS1–M, pTS1–M, and corresponding intermediates are presented in Table 3.

Since TS1–M is a late transition state, the structure and energy of the intermediate C–M is similar to that of TS1–M. Table 3 shows that a new bond in C–M is partially formed: C2–C7 in oC–M and C4–C7 in pC–M. The application of the natural bond order (NBO) analysis<sup>30,31</sup> to the geometry of C–M indicates that hybridization of s and p orbitals for C2 and C4 is very small (20% s and 80% p). The predominant p character of these C atoms with little s mixing indicates that the bonds C2–C7 and C4–C7 are weak. The lengths of C2–C7 and C4–C7 bonds (about 1.72 and 1.78 Å, respectively) are in agreement with the NBO analysis. A consequence of the formation of these weak bonds is that in oC–M the geometry of the benzene ring is slightly deformed in the ortho position, whereas in pC–M the benzene ring is slightly deformed in the positions 1 and 4.

The next step of the reaction is a conversion of the intermediate C–M into D–M via the TS2–M transition state. In both oTS2–M and pTS2–M a new O10–M bond is being formed. In the para route the bond between the O8 and the metal is being broken, whereas in the ortho route the corresponding O8–M bond is not being broken. In oD–M and pD–M the bonds C2–C7 and C4–C7 are almost completely formed, though they are still longer than ordinary single bonds. The NBO analysis of oD–M and pD–M reveals an increase of the contribution of the s orbital in sp hybridization on C2 and C4, so that these carbon atoms are now sp<sup>3</sup> hybridized. The geometry of the intermediate D–M is presented in Table 4.

By inspecting Table 4 one can observe that the O8–Li distance in oD–Li is significantly longer as compared to other O8–M bonds in oD–Ms, implying that the geometry of oD–Li is different from those of other oD–Ms. Actually, the oD–Li geometry corresponds to that of the third intermediate in the carboxylation reaction of sodium



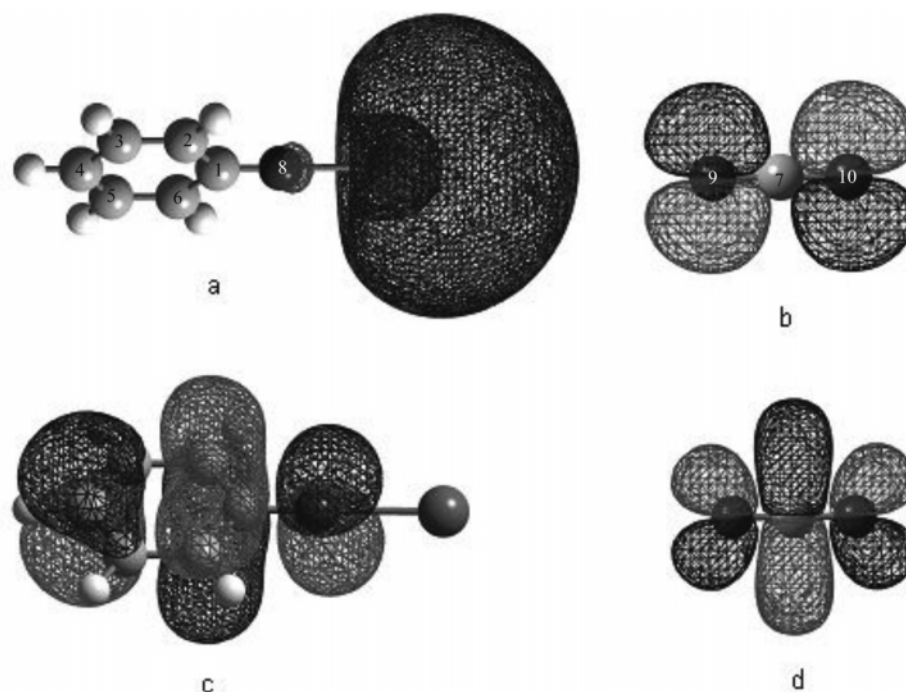


**Figure 3.** (a) LUMO of potassium phenoxide, (b) HOMO of carbon dioxide, (c) HOMO of potassium phenoxide, and (d) LUMO of carbon dioxide.

**Table 2.** APT (Atomic Polar Tensors) Charge Distribution in Reactants and First Intermediate<sup>a</sup>

	PhO–M				B–M			
	Li	K	Rb	Cs	Li	K	Rb	Cs
M	0.89	0.95	0.98	1.02	0.83	0.95	0.97	1.00
O	–1.27	–1.19	–1.18	–1.20	–1.22	–1.22	–1.22	–1.23
o-C	–0.20	–0.25	–0.25	–0.26	–0.13/–0.16	–0.14/–0.17	–0.15/–0.18	–0.16/–0.18
m-C	0.08	0.13	0.14	0.14	0.03/0.01	0.05/0.02	0.05/0.02	0.06/0.03
p-C	–0.22	–0.30	–0.32	–0.33	–0.11	–0.14	–0.14	–0.15

	B–M			
	Li	K	Rb	Cs
carbon dioxide				
C	1.07	1.81	1.81	1.82
O	–0.54	–1.09	–1.09	–1.09
O	–0.54	–0.77	–0.83	–0.84

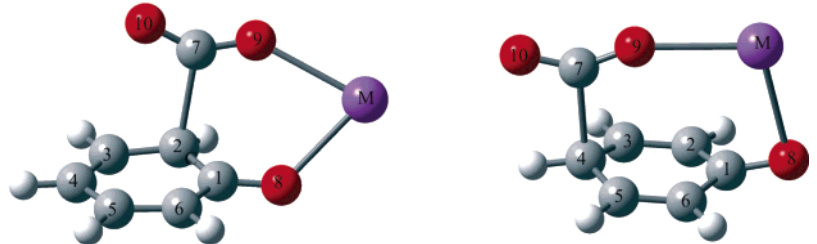
<sup>a</sup> See Figure 2 for definition of symbols.

phenoxide,<sup>17–19</sup> where the metal is chelated with two oxygens. This can be explained with the short ionic radii of lithium and sodium which do not enable the formation of structures where the metal is chelated with three oxygens.

As for the last step of the Kolbe–Schmitt reaction several ways of hydrogen rearrangement are considered. The reactions of homolytic cleavage of the C4–H bond in pD–M and the C2–H bond in oD–M are investigated. The reaction paths are revealed, but the activation energies are very high (about 81 kcal/mol for the cleavage of pD–M and 91 kcal/mol for the cleavage of oD–M). A 1,3 hydrogen shift from C2 to O8 in oD–M occurs with an expectedly high activation energy of 45.34, 42.27, 51.06, and 54.84 kcal/mol for the formation of oTS3–Li, oTS3–K, oTS3–Rb, and oTS3–Cs, respectively. Since in pD–M the distance between the hydrogen bonded to C4 and O8 is too long (4.84 Å in all pD–Ms), a similar 1,5 hydrogen shift from C4 to O8 is not plausible. In addition, a reaction between two pD–M intermediates is not revealed.

On the other hand, the vicinity of electron rich double bond to the hydrogen on C4 indicates that this hydrogen can rearrange from C4 to C3 (or C5). For this reason a migration of hydrogen over the benzene ring is investigated as a plausible last step of the Kolbe–Schmitt reaction in the para position. Since the transformation of pD–M to pE–M exceeds the scope of the present work, the details concerning this step of the Kolbe–Schmitt reaction will be reported elsewhere.

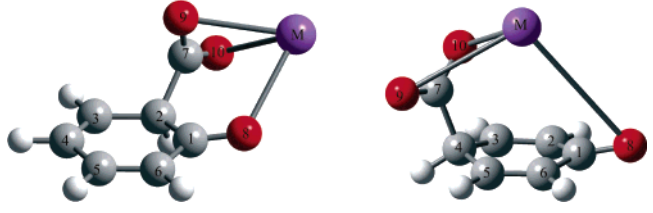
This step of the reaction in both ortho and para positions requires the highest energy barriers, implying that it is the rate limiting step of the Kolbe–Schmitt reaction. These relatively high activation energies are supported by the experimental fact that the reaction mixture has to be heated for 1 h at 150–250 °C under high pressure<sup>7,9,13</sup> in order to form the corresponding salt of hydroxy benzoic acids. Similarly, a 1,3-shift of hydrogen atom in the conversion process for vinyl-acetaldehyde tautomerization requires an activation energy of 56.4 kcal/mol.<sup>35</sup>

**Table 3.** Geometries of oTS1–M (left) and pTS1–M (right) and Bond Lengths for TS1–M and C–M<sup>a</sup>


bond length (Å)	oTS1–Li	oTS1–K	pTS1–K	oTS1–Rb	pTS1–Rb	oTS1–Cs	pTS1–Cs
C2–C7	2.123	2.110		2.097		2.085	
C4–C7			2.085		2.094		2.083
C1–C2	1.459	1.467	1.447	1.469	1.446	1.470	1.447
C1–O8	1.316	1.302	1.305	1.301	1.303	1.299	1.301
O8–M	1.760	2.467	2.640	2.654	2.821	2.847	3.012
M–O9	1.827	2.542	2.557	2.730	2.747	2.925	2.952
O9–C7	1.250	1.247	1.245	1.248	1.243	1.248	1.243
C7–O10	1.214	1.221	1.226	1.223	1.227	1.224	1.229

bond length (Å)	oC–Li	oC–K	pC–K	oC–Rb	pC–Rb	oC–Cs	pC–Cs
C2–C7	1.700	1.720		1.717		1.714	
C4–C7			1.782		1.782		1.787
C1–C2	1.505	1.501	1.476	1.501	1.475	1.458	1.474
C1–O8	1.294	1.296	1.292	1.285	1.291	1.283	1.289
O8–M	1.817	2.537	2.705	2.727	2.897	2.930	3.102
M–O9	1.769	2.468	2.491	2.653	2.673	2.839	2.871
O9–C7	1.290	1.277	1.274	1.276	1.272	1.275	1.270
C7–O10	1.244	1.254	1.247	1.255	1.249	1.257	1.249

<sup>a</sup> See Figure 2 for definition of symbols.**Table 4.** Geometries of oD–M (left) and pD–M (right) and Bond Lengths for TS2–M and D–M<sup>a</sup>


bond length (Å)	oTS2–Li	oTS2–K	pTS2–K	oTS2–Rb	pTS2–Rb	oTS2–Cs	pTS2–Cs
C2–C7	1.563	1.631		1.642		1.653	
C4–C7			1.631		1.638		1.650
C1–C2	1.537	1.518	1.496	1.516	1.496	1.513	1.495
C1–O8	1.279	1.281	1.271	1.281	1.273	1.280	1.275
O8–M	1.972	2.632	4.243	2.814	4.148	3.006	3.958
M–O10	2.390	3.422	3.380	3.636	3.438	3.899	3.510
O10–C7	1.280	1.271	1.272	1.270	1.274	1.270	1.274
C7–O9	1.306	1.289	1.291	1.286	1.288	1.283	1.283
O9–M	1.940	2.568	2.530	2.745	2.751	2.927	3.014

bond length (Å)	oD–Li	oD–K	pD–K	oD–Rb	pD–Rb	oD–Cs	pD–Cs
C2–C7	1.541	1.588		1.599		1.612	
C4–C7			1.564		1.564		1.572
C1–C2	1.539	1.533	1.507	1.530	1.506	1.527	1.505
C1–O8	1.258	1.276	1.266	1.276	1.266	1.275	1.267
O8–M	4.658	2.728	8.155	2.910	8.346	3.114	8.565
M–O10	1.924	2.724	2.610	2.916	2.793	3.121	2.986
O10–C7	1.301	1.287	1.295	1.285	1.294	1.283	1.293
C7–O9	1.307	1.287	1.295	1.285	1.294	1.283	1.293
O9–M	1.928	2.726	2.612	2.899	2.792	3.081	2.986

<sup>a</sup> See Figure 2 for definition of symbols.

## DISTRIBUTION OF PRODUCTS

Our calculations show that the carboxylation reactions of all PhO–Ms occur via similar energetic diagrams. An exception is the reaction of lithium phenoxide with carbon dioxide, where the reaction takes place only in the ortho

position. As an illustration, the energetic profile for the reaction of PhO–K and carbon dioxide is depicted in Figure 4. The relative energies for all intermediates, transition states, and products for the carboxylation reactions of PhO–Ms are given in Table 5.

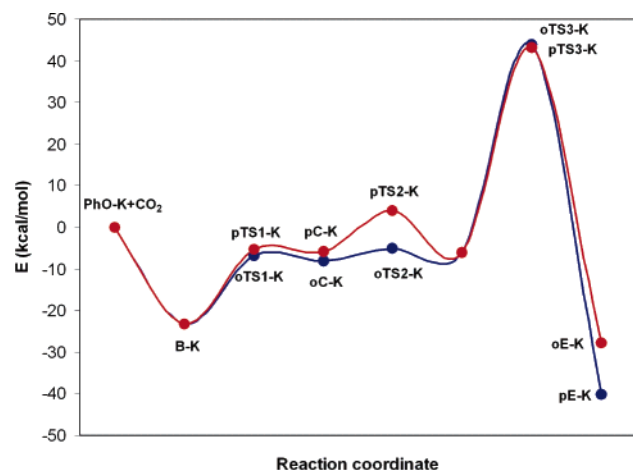


**Figure 4.** Energy diagram for the carboxylation reaction of potassium phenoxide in the ortho (blue line) and para (red line) positions. Energies are calculated relative to reactants. See Figure 2 for definition of symbols.

**Table 5.** Relative Energies in kcal/mol for All Intermediates, Transition States, and Products for the Carboxylation Reactions of All Alkali Metal Phenoxides Considered<sup>a</sup>

M	Li	K	Rb	Cs
B-M	-15.20	-23.25	-21.36	-21.35
oTS1-M	-5.26	-6.78	-4.18	-3.55
pTS1-M		-5.41	-3.87	-4.00
oC-M	-6.92	-8.00	-5.60	-5.06
pC-M		-5.93	-4.79	-4.93
oTS2-M	16.70	-4.98	-3.41	-3.67
pTS2-M		3.96	3.79	1.69
oD-M	10.06	-6.17	-4.41	-4.56
pD-M		-5.98	-4.45	-4.31
oTS3-M	59.40	44.00	50.15	46.66
pTS3-M		43.08	44.99	45.52
oE-M	-29.14	-40.10	-38.35	-38.10
pE-M		-27.79	-25.71	-24.95
ortho/para ratio	1:0	1:0.09	1:0.55	1:2.07

<sup>a</sup> See Figure 2 for definition of symbols. Calculated ratios between the concentrations of the ortho and para products.

Reaction enthalpies and free energies ( $\Delta H^{298}$  and  $\Delta G^{298}$ ) for the carboxylation reactions of all Ph-Ms with carbon dioxide are computed using eqs 1 and 2

$$\Delta H^{298} = H_p^{298} - H_r^{298} \quad (1)$$

$$\Delta G^{298} = G_p^{298} - G_r^{298} \quad (2)$$

where subscripts p and r denote reaction products and reactants. The following results are obtained:  $\Delta H^{298} = -27.57$ ,  $-38.10$  ( $-25.81$ ),  $-35.90$  ( $-23.26$ ), and  $-36.29$  ( $-23.09$ ) kcal/mol for the carboxylation reactions of lithium, potassium, rubidium, and cesium phenoxides, respectively, where the enthalpy values for the reactions in the para position are given in brackets. The  $\Delta G^{298}$  values are 12–13 kcal/mol higher than the corresponding  $\Delta H^{298}$  values. Both reaction enthalpies and free energies indicate that all carboxylation reactions under investigation are exothermic.

According to the Curtin-Hammond principle, the distribution of products is determined with the difference of free energies of the ortho and para transition states. It is clear that the intramolecular conversion of the B-M complex is the most responsible for the products distribution in the

Kolbe-Schmitt reaction. For this reason, the free energy differences between the two transition states for the conversions of B-Ms are calculated. The resulting ratios between the concentrations of the ortho and para products are given in Table 5.

Table 5 shows that the activation energy values for TS1-Ms are mutually very similar, except that of oTS1-Li whose activation energy is lower by 7–8 kcal/mol. The difference between the energies of corresponding oTS1-M and pTS1-M decreases with an increasing atomic number of alkali metal and becomes negative in the case of oTS1-Cs and pTS1-Cs. This is in agreement with the experimental findings claiming that the yield of *p*-hydroxybenzoic acid increases with the increasing atomic number of the alkali metal used.<sup>7,9</sup>

An analysis of the geometries of TS1-Ms reveals that the newly formed C2-C7 and C2-C4 bonds (Table 3) have almost the same lengths in all TS1-Ms, close to 2.1 Å. Also, other corresponding bond lengths are almost identical, with the exception of O-M bonds (bonds O8-M and M-O9 in Table 3). By inspecting these bond lengths one can conclude that both O8-M and M-O9 increase with an increasing ionic radius of alkali metals. This increase of the lengths of bonds O8-M and M-O9 does not affect the geometry of oTS1-M, whereas it is of crucial significance for the pTS1-M geometry. Namely, in pTS1-M these bonds form a bridge that enables the bonding of C7 to the para carbon. Apparently, the geometry of pTS1-M becomes more relaxed as the O-M bond length increases. As an illustration, the geometries of pTS1-K and pTS1-Cs are compared. In pTS1-K C1, C4, and O8 deviate from the plane of the benzene ring by 7°, 8°, and 21°, respectively. In pTS1-Cs these atoms deviate from the plane by 3°, 5°, and 14°.

The ionic radius of lithium is only 0.60, so that a possible geometry of pTS1-Li would require significant deformations of benzene ring. For this reason pTS1-Li does not form, thus explaining the experimental finding that *o*-hydroxybenzoic acid is the only product of the reaction of lithium phenoxide with carbon dioxide.

The intermediate D-M can undergo a reverse reaction forming the intermediate C-M. The energy barriers for the back reactions of the ortho route are very low: 1.19, 1.00, and 0.89 kcal/mol for oTS2-K, oTS2-Rb, and oTS2-Cs, respectively, with an exception of oTS2-Li where this barrier amounts 6.64 kcal/mol. The activation energies for the back reactions of the para route are somewhat higher: 9.94, 8.24, and 6.00 kcal/mol for pTS2-K, pTS2-Rb, and pTS2-Cs, respectively. The intermediate C-M can also undergo a reverse reaction yielding B-M, with the activation energies of 1.66, 1.22, 1.42, and 1.51 kcal/mol for oTS1-Li, oTS1-K, oTS1-Rb, and oTS1-Cs, respectively, and 0.52, 0.92, and 0.93 kcal/mol for pTS1-K, pTS1-Rb, and pTS1-Cs, respectively. These low values of the energy barriers for the back reactions are in agreement with the fact that Kolbe never exceeded the yield of 50% in the reaction of sodium phenoxide with carbon dioxide. By performing the reaction under enhanced pressure (i.e. by shifting the equilibrium to the right side of the reaction) Schmitt improved the yield significantly.<sup>3</sup>

Intermediates C-M and D-M are relatively unstable, and activation energies for their reverse reactions are significantly lower than that of the rate-limiting step. This is in harmony with the experimental results that show that by varying

experimental conditions the ratio of ortho and para products of the Kolbe–Schmitt reaction can be varied.<sup>3,7,8,9</sup>

### CONCLUSIONS

On the basis of the results presented above, one can conclude that the reactions of all PhO–Ms with carbon dioxide occur via very similar reaction mechanisms with similar energy profiles. All reactions are exothermic. The reactions can proceed in the ortho and para positions. The exception is PhO–Li which yields only salicylic acid in the Kolbe–Schmitt reaction. The reaction in both ortho and para positions proceeds via three transition states and three intermediates.

The intramolecular conversion of the intermediate B is most responsible for the product distribution of the Kolbe–Schmitt reaction, since it determines the ortho and para routes of the reaction. The differences in free energies of the corresponding oTS1–Ms and pTS1–Ms result in the ratios of the products concentrations as follows: 1:0 for E–Li, 1:0.0003 for E–Na,<sup>17</sup> 1:0.0941 for E–K, 1:0.5539 for E–Rb, and 1:2.0663 for E–Cs. It is clear that the yield of a para substituted product increases with an increasing ionic radius of the alkali metal used, which is in accord with experimental findings.<sup>7,9</sup> The O–M bond lengths in TS1 also increase with an increasing ionic radius of alkali metals. This is of great importance for the geometry of pTS1–M. Since these bonds form a bridge that enables the bonding of C7 to the para carbon, the geometry of pTS1–M becomes more relaxed as the O–M bond lengths increase.

The ionic radius of lithium is only 0.60, so that a possible geometry of pTS1–Li would require significant deformations of benzene ring. For this reason pTS1–Li does not form. The ionic radius of sodium enables the formation of pTS1–Na but at a very low yield.<sup>6,17–19</sup> As the ionic radius of alkali metals increases, the formation of pTS1–M is more facilitated, and in the case of TS1–Ce the formation of pTS1–Ce is more favorable than that of oTS1–Ce. These computational findings are generally in agreement with experimental results. Our calculations predict salicylic acid as the major product of the carboxylation reaction of PhO–Cs, whereas the experiments showed that the major product of this reaction is *p*-hydroxybenzoic acid.<sup>9</sup>

The last step of the Kolbe–Schmitt reaction is the rate determining step, since both ortho and para routes require relatively high activation energies. Due to low energy barriers for back reactions intermediates D–M and B–M can undergo reverse reactions. It turns out that by varying experimental conditions the ratio of ortho and para products of the Kolbe–Schmitt reaction can be varied.<sup>3,7,8,9</sup>

### ACKNOWLEDGMENT

This work is supported by the Ministry of Science and Environment of Serbia, project no. 142025.

### REFERENCES AND NOTES

- (1) Kolbe, H. Über Synthese der Salicylsäure. *Liebigs Ann.* **1860**, *113*, 125–127.
- (2) Kolbe, H.; Lautemann, E. Über die Constitution und Basicität der Salicylsäure. *Liebigs Ann.* **1860**, *115*, 157–159.
- (3) Schmitt, R. Beitrag zur kenntnis der Kolbe'schen salicylsäure-synthese. *J. Prakt. Chem.* **1985**, *31*, 397.
- (4) Windholz, M. *Salicylic acid*, *The Merck Index*, 10th ed.; Merck & Co. Inc.: Rahway, 1983; p 8190.
- (5) Reynolds J. E. F. Salicylic acid. In *Martindale The Extra Pharmacopoeia*, 31st ed.; The Royal Pharmaceutical Society: London, 1996; pp 1093–1105.
- (6) Baine, O.; Adamson, G. F.; Barton, J. W.; Fitch, J. L.; Swayampati, D. R.; Jeskey, H. A Study of the Kolbe-Schmitt Reaction. II. The Carbonation of Phenols. *J. Org. Chem.* **1954**, *19*, 510–514.
- (7) Lindsey, A. S.; Jeskey, H. The Kolbe-Schmitt Reaction. *J. Chem. Soc.* **1957**, 583–620.
- (8) Wessely, F.; Benedikt, K.; Benger, H.; Friedrich, G.; Prillinger, F. Zur Kenntniss der Carboxylierung von Phenolen. *Monatsh.* **1950**, *81*, 1071–1091.
- (9) Rahim, M. A.; Matsui, Y.; Kosugi, Y. Effects of Alkali and Alkaline Earth Metals on the Kolbe-Schmitt Reaction. *Bull. Chem. Soc. Jpn.* **2002**, *75*, 619–622.
- (10) Lobry de Bruyn, C. A.; Tijmstra, S. Sur le mécanisme de la synthèse de l'acide salicylique. *Rec. Trav. Chim.* **1904**, *23*, 385–393.
- (11) Johnson, J. R. Abnormal reactions of benzylmagnesium chloride. II. The mechanism of the o-tolyl rearrangement. *J. Am. Chem. Soc.* **1933**, *55*, 3029–3032.
- (12) Daives, I. A. Über die Bildung und den Zerfall des Natriumsalicylats. *Z. Phys. Chem. (Muenchen)* **1928**, *134*, 57–86.
- (13) Hales, J. L.; Jones, J. I.; Lindsey, A. S. Mechanism of the Kolbe-Schmitt reaction. I. Infrared studies. *J. Am. Chem. Soc., Abstracts* **1954**, 3145–3151.
- (14) Ayres, D. C. *Carbanions in synthesis*; Oldbourne Press: London, 1966; pp 168–173.
- (15) Kunert, M.; Dinjus, E.; Nauck, M.; Sieler, J. Structure and Reactivity of Sodium Phenoxide – Following the Course of the Kolbe-Schmitt Reaction. *Chem. Ber./Recueil* **1997**, *130*, 1461–1465.
- (16) Kosugi, Y.; Imaoka, Y.; Gotoh, F.; Rahim, M. A.; Matsui, Y.; Sakanishi, K. Carboxylation of Alkali Metal Phenoxides with Carbon Dioxide. *Org. Biomol. Chem.* **2003**, *1*, 817–821.
- (17) Marković, Z.; Engelbrecht, J. P.; Marković, S. Theoretical Study of the Kolbe-Schmitt Reaction Mechanism. *Z. Naturforsch.* **2002**, *57a*, 812–818.
- (18) Stanescu, I.; Achenie, L. E. K. A Theoretical Study of Solvent Effects on Kolbe-Schmitt Reaction Kinetics. *Chem. Eng. Sci.*, accepted for publication.
- (19) Luke, A.; Rishi, G.; Stanescu, I. An in-silico Study of Solvent Effects on The Kolbe-Schmitt Reaction Using a DFT Method. *Mol. Simul.* **2006**, *32*.
- (20) Schrödinger, L. L. C. *Jaguar 4.2 (1991–2002)*; Portland, OR.
- (21) Becke, A. D. Density-functional exchange-energy approximation with correct asymptotic behavior. *Phys. Rev. A* **1988**, 3098–3100.
- (22) Lee, C.; Yang, W.; Parr, R. G. Development of the Colle-Salvetti correlation-energy formula into a functional of the electron density. *Phys. Rev. B* **1988**, 785–789.
- (23) Becke, A. D. Density-functional thermochemistry. II. The role of exact exchange. *J. Chem. Phys.* **1993**, *98*, 5648–5652.
- (24) Frisch, M. J.; Trucks, G. W.; Schlegel, H. B.; Scuseria, G. E.; Robb, M. A.; Cheeseman, J. R.; Zakrzewski, V. G.; Montgomery, J. A. Jr.; Stratmann, R. E.; Burant, J. C.; Dapprich, S.; Millam, J. M.; Daniels, A. D.; Kudin, K. N.; Strain, M. C.; Farkas, O.; Tomasi, J.; Barone, V.; Cossi, M.; Cammi, R.; Mennucci, B.; Pomelli, C.; Adamo, C.; Clifford, S.; Ochterski, J.; Petersson, G. A.; Ayala, P. Y.; Cui, Q.; Morokuma, K.; Malick, A. D.; Rabuck, K. D.; Raghavachari, K.; Foresman, J. B.; Cioslowski, J.; Ortiz, J. V.; Baboul, A. G.; Stefanov, B. B.; Liu, G.; Liashenko, A.; Piskorz, P.; Komaromi, I.; Gomperts, R.; Martin, R. L.; Fox, D. J.; Keith, T.; Al-Laham, M. A.; Peng, C. Y.; Nanayakkara, A.; Challacombe, M.; Gill, P. M. W.; Johnson, B.; Chen, W.; Wong, M. W.; Andres, J. L.; Gonzalez, C.; Head-Gordon, M.; Replogle, E. S.; Pople, J. A. *Gaussian 98, Revision A.9*; Gaussian, Inc.: Pittsburgh, PA, 1998.
- (25) *Chemical Applications of Density Functional Chemistry*; Laird, A., Ross, R. B., Zeigler, T., Eds.; American Chemical Society: Washington, DC, 1996.
- (26) Hay, P. J.; Wadt, W. R. Ab initio effective core potentials for molecular calculations. Potentials for the transition metal atoms Sc to Hg. *J. Chem. Phys.* **1985**, *82*, 270–283.
- (27) Wadt, W. R.; Hay, P. J. Ab initio effective core potentials for molecular calculations. Potentials for main group elements Na to Bi. *J. Chem. Phys.* **1985**, *82*, 284–298.
- (28) Hay, P. J.; Wadt, W. R. Ab initio effective core potentials for molecular calculations. Potentials for K to Au including the outermost core orbitals. *J. Chem. Phys.* **1985**, *82*, 299–310.
- (29) Dunning, T. H., Jr.; Hay, P. J. *Modern Theoretical Chemistry*; Schaefer, H. F., Ed.; Plenum: New York, 1976; Vol. 3.
- (30) Foster, J. P.; Weinhold, F. Natural hybrid orbitals. *J. Am. Chem. Soc.* **1980**, *102*, 7211–7218.
- (31) Reed, A. E.; Weinstock, R. B.; Weinhold, F. Natural population analysis. *J. Chem. Phys.* **1985**, *83*, 735–746.



- (32) Schaftenaar, G. *MOLDEN 3.7*; CAOS/CAMM Center: The Netherlands, 1998.
- (33) Hehre, W. J.; Shusterman, A. J.; Huang, W. W. *A Laboratory Book of Computational Organic Chemistry*; Wavefunction, Inc.: Irvine, CA, 1996.
- (34) Marti, J. A new method for assessing similarities among atoms in molecules. *Chem. Phys.* **2001**, 265, 263–272.
- (35) Suenobu, K.; Nagaoka, M.; Yamabe, T. The faster conversion of ethene thiol than vinyl alcohol in tautomerization reactions in aqueous solution — theoretical prediction *J. Mol. Struct. (THEOCHEM)* **1999**, 461–462, 581–588.

CI0600556